

# 1 **Estimating aquifer thickness using multiple pumping tests**

2 Jean-Christophe Maréchal<sup>a,b,c,d\*</sup>, Jean-Michel Vouillamoz<sup>a,e</sup>, M.S. Mohan Kumar<sup>a,f</sup>, Benoit  
3 Dewandel<sup>g</sup>

4

5 <sup>a</sup> Indo-French Cell for Water Sciences, IISc-IRD Joint laboratory, Indian Institute of Science,  
6 560 012 Bangalore, India

7 <sup>b</sup> Université de Toulouse ; UPS (OMP) ; LMTG; 14 Av Edouard Belin, F-31400 Toulouse,  
8 France

9 <sup>c</sup> CNRS ; LMTG ; F-31400 Toulouse, France

10 <sup>d</sup> IRD ; LMTG ; F-31400 Toulouse, France

11 <sup>e</sup> LTHE, IRD, BP 53, 38041 Grenoble cedex 9, France

12 <sup>f</sup> Department of Civil Engineering, Indian Institute of Science, 560 012 Bangalore, India

13 <sup>g</sup> brgm, 1039 rue de Pinville, 34000 Montpellier, France

14

## 15 **Abstract**

16 A method to estimate aquifer thickness and hydraulic conductivity has been developed,  
17 consisting of multiple pumping tests. The method requires short-duration pumping cycles on  
18 an unconfined aquifer with significant seasonal water-table fluctuations. The interpretation of  
19 several pumping tests at a site in India under various initial conditions provides information  
20 on the change in hydrodynamic parameters in relation to the initial water-table level. The  
21 transmissivity linearly decreases compared with the initial water level, suggesting a  
22 homogeneous distribution of hydraulic conductivity with depth. The hydraulic conductivity is  
23 estimated from the slope of this linear relationship. The extrapolation of the relationship  
24 between transmissivity and water level provides an estimate of the aquifer thickness that is in  
25 good agreement with geophysical investigations. The hydraulically active part of the aquifer

26 is located in both the shallow weathered and the underlying densely fractured zones of the  
27 crystalline basement. However, no significant relationship is found between the aquifer  
28 storage coefficient and initial water level. This new method contributes to filling the  
29 methodological gap between single pumping tests and hydraulic tomography, in providing  
30 information on the variation of the global transmissivity according to depth. It can be applied  
31 to any unconfined aquifer experiencing large seasonal water-table fluctuations and short  
32 pumping cycles.

33

34 Keywords: groundwater hydraulics, India, crystalline rocks, fractured rocks, hydraulic testing

35

## 36 **1. Introduction**

37 Solving the inverse problem of common pumping test interpretation leads to the  
38 determination of the product of the hydraulic conductivity  $K$  by the initial saturated thickness  
39  $b$  of the aquifer. This is the case in both confined (Theis 1935) or unconfined aquifer models  
40 (Neuman 1975). The solution of the problem is non unique and an infinite set of  $K - b$   
41 couples leads to the same transmissivity value  $T = K b$ . Therefore, additional information is  
42 required in order to solve the nonuniqueness of the solution.

43 In sedimentary rocks, the saturated thickness of the aquifer can be deduced from the  
44 geological log obtained during well drilling as hydrogeologic units can be defined from  
45 drilling cuttings or cores. In fractured crystalline rocks, the concept that groundwater flows  
46 mainly occur in a shallow higher-permeability zone (“active” zone) that overlies a deeper  
47 lower-permeability zone hosting little flow (“inactive” zone) is documented in mountainous  
48 regions (Mayo et al. 2003) and in flat bedrock areas (Davis and Turk 1964; Dewandel et al.  
49 2006; Maréchal et al. 2004). The thickness of this more permeable layer is not well known as  
50 information from drilling does not always provide accurate indicators on the vertical

51 extension of conductive fractures. Flowmeter measurements can provide information on the  
52 location of conductive fractures (Maréchal et al. 2004) but they can rarely be extended to a  
53 larger scale beyond the close vicinity of the well, except in cross-borehole flow logs (Paillet  
54 1998). Comprehensive geophysical measurements, including appropriate borehole logging,  
55 are rarely carried out for small-scale groundwater development projects because such  
56 techniques are costly. However, the well-known and easy to implement rock electrical  
57 resistivity measurement (both logging in wells and measurements from the surface) can  
58 provide indirect information on the extension of the weathered/fissured and fractured zones  
59 (Chapellier 1987). Unfortunately, electrical resistivity measurements can hardly differentiate  
60 hydraulically active zones from clay-bearing ones.

61         Recently, the hydraulic tomography has been developed in order to improve the  
62 uniqueness of the inverse solution and reduce uncertainties in the identified hydraulic  
63 property field (Buttler et al. 1999; Gottlieb and Dietrich 1995). This method implies injection  
64 or pumping at various depths and various wells (i.e. sequential pumping tests) in order to  
65 provide additional information. If this new technique looks promising, it needs extensive field  
66 experiments and data processing for data inversion. The objective of the present paper is to  
67 explore the methodological gap between the common single pumping test modeled using  
68 classical Theis and Neuman models (whose results are strongly non-unique) and the hydraulic  
69 tomography method (whose application requires large investment).

70         Multiple pumping tests applied to the same unconfined aquifer using the same  
71 pumping and observation wells under various initial conditions are investigated. The  
72 complexity of periodic pumping with variable duration induces complicated signals which  
73 depend on the pumping history (Bangoy and Drogue 1994). Existing interpretation methods  
74 (i.e. Birsoy and Summers 1980) are valid for confined aquifers only. In this paper, one way of

75 interpretation of such a data series is proposed for an unconfined aquifer. It is applied on a  
76 shallow fractured crystalline aquifer.

77

## 78 **2. Study area**

79         The numerous power cuts in rural India lead to the existence of daily pumping cycles  
80 in irrigation and village wells (Maréchal et al. 2006). The study site consists of two wells  
81 located in the Maddur watershed (south of Gundlupet), a rural area of south Karnataka, India  
82 (Figure 1). The geology belongs to the Precambrian Dharwar supergroup (Moyen et al. 2001)  
83 and consists of gneiss with amphibolites and quartz dykes. The pumping well (PW) provides  
84 domestic water to the village of Chenmallipur. Water is pumped every day using a  
85 submersible pump at the constant pumping rate,  $Q = 2.2 \pm 0.2$  l/s. Abandoned well CMP1  
86 constitutes an observation well located 66 meters away from PW. These wells can be  
87 considered as fully penetrating, as their depths ( $> 50$  and  $72$  meters, Table 1) are larger than  
88 the depth to the bottom of the fractured-weathered zone which is usually about  $30 - 50$  meters  
89 in this geological context (Table 1).

90

91 The weathering profile of the gneissic hard-rock is constituted from the top to bottom by  
92 (Figure 2):

- 93         - A clayey-sandy saprolite, derived from prolonged in situ decomposition of bedrock, of  
94             1- 2 meters thickness;
- 95         - A weathered and fractured layer which is generally characterized by a dense  
96             horizontal fissuring in the first few meters and a depth-decreasing density of fractures  
97             (Houston and Lewis 1988; Howard et al. 1992). Its thickness is unknown but it hardly  
98             ever exceeds tens of meters.

99 - The fresh basement which is permeable only where tectonic fractures are present. At  
100 the catchment scale, this layer is generally considered as impermeable and of very low  
101 porosity (Maréchal et al. 2004).

102 The water table fluctuates between 3 and 25 meters depth, thus only within the fractured  
103 layer. It is therefore not restricted by any confining layer above it. The aquifer is a priori  
104 unconfined and bounded below by the fresh basement (aquiclude). The saturated thickness is  
105 not known.

106 Electrical resistivity tomography (ERT) has been carried out (location at Figure 1) to check  
107 the bottom of the weathered zone. A Wenner alpha array was implemented with 64 electrodes  
108 and an inter-electrode spacing of 4 meters in 2008. The inversion fits well with the calculated  
109 apparent resistivity data with a root mean square (RMS) of 2.2% (Figure 3).

110 The geological structure is homogeneous and relatively flat at the scale of the ERT, thus  
111 confirming that the use of a homogeneous analytical solution to interpret the pumping tests is  
112 appropriate. The depth to the bottom of the weathered rock is estimated with the 400 - 600  
113  $\Omega\text{m}$  isocontour as calculated by Braun et al. (2009) and Descloitres et al. (2008) in a  
114 neighboring site. It ranges from 18 to 25 meters below ground surface. Resistivity values  
115 higher than 400 to 600  $\Omega\text{.m}$  are interpreted as fresh or fractured rock.

116 To assess if a fractured zone that can not be identified by the ERT is present below the  
117 isocontour of 400 - 600  $\Omega\text{.m}$ , borehole electrical logging was carried out in CMP1 (Figure 4).

118 The three normal probe (NL) measurements clearly reveal an interface at 19 meters below  
119 ground surface. Looking at the normal probe (NL) of 64 cm length that is less sensitive than  
120 the shorter probes to the groundwater resistivity, the values of apparent resistivity indicate  
121 weathered or fissured saturated rocks between the static water level (SWL) and 19 meters  
122 depth. This depth is in good agreement with that obtained from the ERT. Below 19 meters,  
123 the apparent resistivity ranges between 500 and 1000  $\Omega\text{.m}$ , thus indicating a fracture zone that

124 extends down to 31 meters. At greater depths, apparent resistivity values over 1000  $\Omega\text{m}$   
125 indicate not fractured basement rocks.

126 The duration of pumping cycles is determined by measuring the temperature of the outlet pipe  
127 of the pumping well (Massuel et al. 2009). The contrast between air and groundwater  
128 temperatures allows for identification of when the pumping starts and stops. A pumping phase  
129 is characterized by a steady temperature value close to groundwater temperature. A  
130 Thermochron iButton temperature logger with a time-step interval of 5 minutes was used at  
131 the pumping well. The discharge of the well was measured several times during the  
132 experiment in order to verify its constancy. The observation well was monitored using a water  
133 level data logger with a 10 minute time-step. Therefore, this set of wells constitutes a small  
134 autonomous experimental ‘laboratory’ for the analysis of multiple pumping tests. Pumping  
135 cycles analyzed in this study were selected at least 5 days after the last rainfall event in order  
136 to avoid any drainage effects.

137

### 138 **3. Method**

#### 139 ***3.1. Multiple pumping tests in unconfined aquifer***

140 When drawdown values in unconfined aquifers are plotted versus logarithm of time, they  
141 delineate an S-shape curve consisting of a steep segment at early times, a flat segment at  
142 intermediate times and a steeper segment at later times. This is caused by the delayed water-  
143 table response of the unconfined aquifer. Initially developed by Boulton [1970], the theory of  
144 “‘delayed yield from storage in unconfined aquifers’” [Boulton and Pontin, 1971] was used by  
145 Neuman (1975) to develop an analytical solution adapted to anisotropic unconfined aquifers,  
146 where  $K_r$  is the radial horizontal permeability and  $K_z$  is the vertical permeability ( $K_r = K_z$  in  
147 the isotropic case). The Neuman model considers an infinite unconfined homogeneous aquifer  
148 with an initial saturated thickness  $b$ . When a complete well is pumped at a constant discharge

149 rate  $Q$ , one part of the water comes from elastic storage in the aquifer and the other from  
 150 gravitational drainage at the free surface (specific yield). The Neuman solution, plotted on  
 151 type curves, provides reduced drawdowns  $s_D$  in an observation well located at a radial  
 152 distance  $r$  from the pumping well,  $s_D = 4\pi T s / Q$  as a function of (a) reduced time  $t_s = Tt / S r^2$   
 153 for a series of “type A” curves (Neuman 1975) at early times; and (b) reduced time  
 154  $t_y = Tt / S_y r^2$  for a series of “type B” curves at late times, where  $T = K_r b$  ( $T$  is the  
 155 transmissivity of the aquifer),  $S$  is the storage coefficient,  $S_y$  is the specific yield,  $t$  is the time  
 156 since the start of pumping, and  $s$  is the drawdown. Therefore, matching a type A curve on  
 157 measured drawdown at early times leads to the estimate of  $S$ , while a type B curve at late  
 158 times leads to  $S_y$ .

159 The storage coefficient matched on the type A curve can be written as

$$160 \quad S = S_s b = \gamma(\alpha + \phi\beta)b \quad (1)$$

161 where  $\gamma = 9.789 \times 10^3 \text{ N/m}^3$  ( $\gamma$  is the specific weight of water at 20°C),  $\alpha$  is the  
 162 compressibility of the rock,  $\beta = 4.4 \times 10^{-10} \text{ m}^2/\text{N}$  ( $\beta$  is the compressibility of water) and  $\phi$  the  
 163 porosity of the rock.

164 In an unconfined aquifer, the transmissivity varies with the saturated thickness of the aquifer  
 165  $b$ . Therefore, the interpretation of  $n$  pumping tests conducted with various saturated aquifer  
 166 thickness  $b_i$  leads to  $n$  values of the transmissivity  $T_i = K_r b_i$ , for  $i = 1, 2, \dots, n$ . The  
 167 interpretation of multiple pumping tests precisely relies on the analysis of the relationship  
 168 between  $K_r b_i$  and  $b_i$  (Figure 5).

169  
 170 Let us consider a homogeneous and isotropic unconfined aquifer with a maximum saturated  
 171 thickness equal to  $b_{max}$  (corresponding to a minimum depth to water table  $d_{min}$ ) measured after  
 172 a long recharge period (Figure 5a); the transmissivity at that time is equal to  $K_r b_{max}$ . During

173 the dry season, the water table declines and the transmissivity decreases to  $K_r b_{min}$  along with  
174 the saturated thickness from  $b_{max}$  to  $b_{min}$ . A series of pumping tests conducted at various dates  
175 during this period leads to a transmissivity ranging from  $K_r d_{max}$  to  $K_r d_{min}$ . The  $n$  plots of  
176 estimated transmissivity according to the initial water-table depth should align along a straight  
177 line with a slope inversely equal to the horizontal hydraulic conductivity  $K_r$  of the aquifer  
178 (Figure 5b). The intercept of this straight line with the ordinates axis corresponds to the depth  
179  $d_0$  for which  $K_r b = 0$ , corresponding to the bottom of the aquifer.

180 Multiple pumping tests carried out on the same borewell are rare, costly and difficult to  
181 implement. However pumping cycles induced by irrigation or drinking water supply wells can  
182 be easily monitored using automatic water level recorders installed in close observation wells.  
183 These intermittent pumping tests constitute an interesting and low-cost alternative technique  
184 to conducting multiple pumping tests. The multiple pumping tests method can then be applied  
185 in any region of the world with significant seasonal water table fluctuations (due to seasonal  
186 rainfall during monsoon for example) and relatively short water pumping cycles.

187

### 188 **3.2. Drawdown correction**

189 Under daily pumping cycles, the short duration of the recovery phase does not allow  
190 the system to recover to a static state before the next pumping phase. Therefore, the effect of  
191 previous pumping phases on the drawdown should be taken into account. Two methods have  
192 been tested for that purpose. The first method consists of interpreting several pumping and  
193 recovery phases using the superposition principle (Bangoy and Drogue 1994) in order to  
194 minimize the effect of non static initial conditions. However, increasing the duration of the  
195 interpretation window induces an increasing effect on the existing trends, i.e. depletion trend  
196 during dry season or increasing trend during monsoon. This leads to an overestimate of the  
197 transmissivity during the monsoon and to an underestimate during the dry season. Therefore,

198 an alternative technique has been applied. For each pumping phase, the measured drawdown  
 199 has been corrected from the previous recovery phase as illustrated in Figure 6. The correction  
 200 involves computing the drawdown with respect to the water level that would have been  
 201 measured if the pumping had not have taken place (real drawdown), and not with respect to  
 202 the initial water level (apparent drawdown). In order to reconstruct what would have been the  
 203 water level, the previous recovery is extrapolated using an observed reference recovery  
 204 (Figure 6). Then the real drawdown is computed, adding to the observed drawdown the  
 205 remaining recovery  $\Delta s(t)$  which increases from 0 (at the beginning of the pumping phase,  
 206 Figure 6) to  $\Delta s_{\max}$  (at the end):

$$207 \quad s'(t) = s(t) + \Delta s(t) \quad (1)$$

208 where  $s(t)$  is the observed apparent drawdown and  $s'(t)$  is the real drawdown corrected from  
 209 the previous recovery phase. This technique is actually an application of the superposition  
 210 principle valid for linear systems, which is not the case for an unconfined aquifer. Therefore  
 211 the error introduced by this assumption on hydrodynamic parameters estimation should be  
 212 computed. Practically, this error arises from the drawdown correction  $\Delta s(t)$  ( $0 < \Delta s(t) < \Delta s_{\max}$ )  
 213 which contradicts the hypothesis of a constant aquifer thickness. Therefore the maximum  
 214 uncertainty on estimated  $\hat{K}_r b$  is

$$215 \quad \frac{\hat{K}_r b}{K_r b} = \frac{K_r (b + \Delta s_{\max})}{K_r b} = 1 + \frac{\Delta s_{\max}}{b} \quad (2)$$

216 where  $\hat{K}_r b$  is the transmissivity estimated after drawdown correction and  $K_r b$  the  
 217 transmissivity that would have been obtained if no correction was necessary. The same  
 218 uncertainty  $\Delta s_{\max}$  has been applied to the initial water-table depth. However, pumping tests  
 219 occurring after a recovery phase longer than 24 hours were not corrected as the water level

220 reached its initial level: the uncertainty is nil for these cases. Uncertainties are represented by  
221 errors bars in Figures 10 and 11.

222

## 223 **4. Results**

224 The water-table fluctuations at well CMP1 during the monitoring period (January  
225 2007 to August 2008) are presented Figure 7. The analysis of water-level signal leads to the  
226 identification of two components. The trends of high amplitude are linked to the sequence of  
227 dry and rainy seasons caused by the monsoon regime. Water-level fluctuations of lower  
228 amplitude (and higher frequency) are caused by short pumping cycles. The trend in water-  
229 table depth (between 2 and 25 meters below the surface) lends itself to being regarded as the  
230 initial water levels of short pumping cycles. This is precisely the needed condition for the  
231 application of the multiple pumping tests method described in this paper: existence of short  
232 duration pumping cycles on an aquifer with seasonal high amplitude water-table fluctuations.  
233 Consequently, each pumping cycle (identified by a serial number at Figure 7) can be  
234 interpreted as an individual short duration pumping test with varying initial conditions.

### 235 **4.1 Correction of the measured drawdown**

236 The reference recovery scenario used for correcting the recorded drawdown is the 19  
237 hours-long recovery observed between 19th and 20th August 2008. This reference was chosen  
238 as it is the longest recovery recorded during the observation period and because it is located at  
239 an average water-table depth. The recovery correction was independently applied to each  
240 pumping test according to the duration of the previous pumping phase. Comparison between  
241 several pumping tests (a, b, c, d and e, see Figure 8 for the dates) with close initial water  
242 levels and different previous recovery phases shows that the corrected drawdowns are very  
243 similar (Figure 8). The difference compared with uncorrected apparent drawdown is about 22

244 % . The coefficient of variation  $CV$  of the corrected drawdown has been computed at every  
 245 time step  $t$  as the ratio:

$$246 \quad CV(t) = \frac{\sigma(s'_a(t), s'_b(t), s'_c(t), s'_d(t), s'_e(t))}{\mu(s'_a(t), s'_b(t), s'_c(t), s'_d(t), s'_e(t))} \quad (3)$$

247 with  $\sigma$  the standard deviation and  $\mu$  the average of corrected drawdown  $s'$  during  
 248 pumping tests a, b, c, d and e at time  $t$ .  $CV$  tends to quickly decrease and becomes inferior to  
 249 10 % at early times ( $> 2\,500$  s, Figure 8). This shows that the effects of previous recovery  
 250 phases have been successfully corrected. It also suggests a very good repeatability of pumping  
 251 cycle results.

252

#### 253 **4.2 Interpretation of the corrected drawdown**

254 The drawdown derivatives (diagnostic plot) of four pumping cycles and one recovery with  
 255 variable initial conditions are compared in Figure 9.

256 The equation used to calculate the drawdown derivative at the point of interest,  $i$ , is (Bourdet  
 257 et al. 1989):

$$258 \quad \left( \frac{ds'}{dX} \right)_i = \frac{\left( \frac{\Delta s'_1}{\Delta X_1} \Delta X_2 + \frac{\Delta s'_2}{\Delta X_2} \Delta X_1 \right)}{\Delta X_1 + \Delta X_2} \quad (4)$$

259 where 1= point before  $i$ , 2 = point after,  $X$  is time function ( $\ln \Delta t$ ), and  $s'$  is the corrected  
 260 drawdown. Noise effects are reduced by choosing the points 1 and 2 where the derivative is  
 261 calculated sufficiently distant from point  $i$ .

262 Figure 9 does not show the U-shape curve typical of delayed yield response of the unconfined  
 263 aquifer. This is due to the relative short duration of the pumping cycles and the quite long  
 264 distance between observation and pumping wells. In Fig 9 the general trend is a stabilization  
 265 of the derivative, corresponding to the early-times type A curve of the Neuman model.

266 One can also observe that the deeper the initial water level, the higher the derivative plateau  
267 (Figure 9). This shows a decrease of the transmissivity with the water-table decline since  
268  $K_r b$  can directly be estimated from the derivative plateau (Chow 1952):

$$269 \quad \frac{\partial s'}{\partial \ln(t)} = \frac{Q}{4\pi K_r b} \quad (6)$$

270  
271  
272 Drawdown matches successfully the type A curves of the Neuman model for early times as  
273 suggested by the diagnostic plot. The results of the interpretation of  $n = 24$  pumping phases  
274 between January 2007 and August 2008 for CMP1 are given at **Erreur ! Source du renvoi**  
275 **introuvable..**

276

## 277 **5. Discussion**

### 278 **5.1. Hydraulic conductivity and aquifer thickness**

279 Within the investigated range of water-level depths ( $3.45 < d_i < 20.63$  m), the  
280 calculated transmissivity  $T_i = K_r b_i$  (for  $i = 1$  to 24) reasonably matches a linear relationship  
281 with the initial depth to water level  $d_i$  (Figure 10). The deeper initial water level gives the  
282 lower value of transmissivity. The observed linear relationship suggests that the horizontal  
283 hydraulic conductivity  $K_r$  is constant with depth. Hydraulic conductivity  $K_r$  can be calculated  
284 as the inverse slope of the fitted line as suggested earlier in Figure 5b. One linear regression is  
285 calculated (Figure 10): the inverse slope of the linear regression is  $K_r = 3.1_{-0.7}^{+1.4} \times 10^{-6}$  m/s  
286 (correlation coefficient  $R = 0.83$ ). This value is similar to other results obtained for the Indian  
287 Shield from slug tests ( $K = 4.4 \times 10^{-6}$  m/s, Maréchal et al. 2004) and pumping tests ( $K = 1 \times$   
288  $10^{-5}$  m/s, Maréchal et al. 2004). The extrapolation of this linear relationship for  $K_r b = 0$   
289 provides the depth at which  $b = 0$ , that is the depth to the bottom of the aquifer  $d_0 = 26.9 \pm 4.5$   
290 m (Figure 10).

291

## 292 **5.2. Specific storage**

293 No clear relationship appears between calculated storage  $S_s b_i$  and the water-table depth  
294 (Figure 11). However, the obtained values range from  $1.4 \times 10^{-4}$  to  $3.6 \times 10^{-4}$  and are close to  
295 the mean storage value obtained for the Indian Shield for granite ( $4.8 \times 10^{-4}$ , Maréchal et al.  
296 2004). Assuming  $\phi \approx 0.02$  (Maréchal et al. 2006) in Eq. (1),  $\alpha = 10^{-9} \text{ m}^2/\text{N}$  (ranging from  $10^{-8}$   
297 to  $10^{-10}$  for fractured rock according to Kruseman and Ridder (1990)) and  $b = 20 \text{ m}$ , one  
298 obtains  $S = 2 \times 10^{-4}$  which is very close to the values obtained using the Neuman model on  
299 drawdown curves of short duration pumping tests. It is clear that the short duration pumping  
300 tests do not lead to the estimate of specific yield but rather to the estimate of elastic storage.  
301 Longer duration pumping tests are needed to determine the specific yield  $S_y$  of the aquifer  
302 using the delayed yield approach (Neuman 1975).  
303 The lack of linear relationship between storage and water-table depth suggests that the  
304 specific storage is not homogeneous in this aquifer. As a consequence, the hydraulic  
305 diffusivity ( $T/S$ ) is not constant as well.

## 306 **5.3. Comparison with geophysical data**

307 Geophysical measurements suggest that the rock is weathered and highly fractured down to  
308 19 meters below ground surface, and then the rock is moderately fractured down to 31 meters  
309 deep. This result is in good agreement with the depth to the bottom of the aquifer obtained  
310 from the pumping test analysis ( $d_0 = 26.9 \pm 4.5 \text{ m}$ ). It suggests that the hydraulically active  
311 part of the aquifer is only located in the shallow weathered and densely fractured zones of the  
312 crystalline basement (Maréchal 2009). This result also confirms other findings obtained in  
313 crystalline aquifers from Africa (Chilton and Foster 1995; Houston and Lewis 1988; Taylor

314 and Howard 2000), the United States (Davis and Turk 1964) and India (Dewandel et al. 2006;  
315 Maréchal et al. 2004).

316

## 317 **6. Conclusion**

318 Multiple pumping tests carried out on the same unconfined aquifer under various initial  
319 conditions (initial water level) allow characterization of various responses of the system.  
320 Interpretation of short-duration pumping phases shows that the transmissivity decreases  
321 linearly with the increase of water-table depth. The extrapolation of this linear relation allows  
322 for estimation of the aquifer thickness. The main advantage of this method is that it provides  
323 the thickness of the really hydraulically active part of the aquifer. For the analyzed data set,  
324 the obtained thickness is consistent with the local thickness of weathered fractured rocks  
325 estimated using geophysical methods.

326 The main limitation of this method is that it requires high amplitude seasonal water-level  
327 fluctuations. This method can be applied to other types of unconfined aquifer, for example,  
328 aquifers present in sedimentary rocks. The use of longer pumping cycles would allow for  
329 estimation of the total set of hydrodynamic parameters, including specific yield and the  
330 permeability anisotropy ratio of the unconfined aquifer.

331

## 332 **Acknowledgments**

333 The Maddur Basin study is part of the ORE-BVET project (Observatoire de Recherche en  
334 Environnement – Bassin Versant Expérimentaux Tropicaux). Apart from specific support  
335 from the French Institute of Research for Development (IRD), the Embassy of France in India  
336 and the Indian Institute of Science, our project benefited from funding from IRD and  
337 INSU/CNRS (Institut National des Sciences de l'Univers / Centre National de la Recherche  
338 Scientifique) through the French programmes ECCO-PNRH (Ecosphère Continentale:

339 Processus et Modélisation – Programme National Recherche Hydrologique) and EC2CO  
340 (Ecosphère Continentale et Côtière). It is been funded by IFCPAR (Indo-French Center for  
341 the Promotion of Advanced Research W-3000) and supported by ANR (National Research  
342 Agency, France) under VMCS Programme No ANR-08-VULN-010-03/SHIVA. The  
343 multidisciplinary research carried out on the Maddur watershed began in 2005 under the  
344 control of the IISc/IRD laboratory IFCWS (Indo-French Cell for Water Sciences). The  
345 authors warmly thank M. Sekhar, S. Subramanian and J.J. Braun for their support. The  
346 contribution of Associate Editor Nadim Copty and Thomas Graf was highly appreciated.

347

## 348 **References**

349

350 Bangoy, L.M. and Drogue, C., 1994. Analysis of intermittent pumping tests in fissured fractal  
351 aquifers: theory and applications. *Journal of Hydrology*, 158(1-2): 47-59.

352 Birsoy, Y.K. and Summers, W.K., 1980. Determination of Aquifer Parameters from Step  
353 Tests and Intermittent Pumping Data. *Ground Water*, 18(2): 137-146.

354 Boulton, N. S. (1970), Analysis of data from pumping tests in unconfined anisotropic  
355 aquifers, *Journal of Hydrology*, 10, 369–378.

356 Boulton, N. S., and J. M. A. Pontin (1971), An extended theory of delayed yield from storage  
357 applied to pumping tests in unconfined anisotropic aquifers, *Journal of Hydrology*, 14,  
358 53–65.

359 Bourdet, D., Ayoub, J.A. and Pirard, Y.M., 1989. Use of pressure derivative in well-test  
360 interpretation. *SPE Formation Evaluation*, 4(2): 293-302.

361 Braun, J.J., Descloitres, M., Riotte, J., Fleury, S., Barbiero, L., Boeglin, J.L., Violette, A.,  
362 Lacarce, E., Ruiz, L., Sekhar, M., Kumar, M.S.M., Subramanian, S. and Dupree, B.,  
363 2009. Regolith mass balance inferred from combined mineralogical, geochemical and  
364 geophysical studies: Mule Hole gneissic watershed, South India. *Geochimica Et*  
365 *Cosmochimica Acta*, 73(4): 935-961.

366 Butler, J.J., Jr., McElwee, C.D. and Bohling, G.C., 1999. Pumping tests in networks of  
367 multilevel sampling wells: Motivation and Method. *Water Resources Research*,  
368 35(11): 3553-3560.

369 Chapellier, D., 1987. *Diagraphies appliquées à l'hydrologie [Wells logging applied to*  
370 *hydrology]*. Lavoisier, Paris.

371 Chilton, P.J. and Foster, S.S.D., 1995. Hydrogeological characteristics and water-supply  
372 potential of basement aquifers in Tropical Africa. *Hydrogeology Journal*, 3(1): 3-49.

373 Chow, V.T., 1952. On the determination of transmissibility and storage coefficients from  
374 pumping test data. *Trans Am Geophys Union*, 33: 397-404.

375 Davis, S.N. and Turk, L.J., 1964. Optimum depth of wells in crystalline rocks. *Groundwater*,  
376 2(2): 6-11.

377 Descloitres, M., Ruiz, L., Sekhar, M., Legchenko, A., Braun, J.J., Mohan Kumar, M.S. and  
378 Subramanian, S., 2008. Characterization of seasonal local recharge using electrical  
379 resistivity tomography and magnetic resonance sounding. *Hydrological Processes*,  
380 22(3): 384-394.

381 Dewandel, B., Lachassagne, P., Wyns, R., Marechal, J.C. and Krishnamurthy, N.S., 2006. A  
382 generalized 3-D geological and hydrogeological conceptual model of granite aquifers  
383 controlled by single or multiphase weathering. *Journal of Hydrology*, 330(1-2): 260-  
384 284.

385 Gottlieb, J. and Dietrich, P., 1995. Identification of the permeability distribution in soil by  
386 hydraulic tomography. *Inverse Problem*, 11: 353-360.

387 Houston, J.F.T. and Lewis, R.T., 1988. The Victoria Province Drought Relief Project, II.  
388 Borehole Yield Relationships. *Ground Water*, 26(4): 418-426.

389 Howard, K.W.F., Hughes, M., Charlesworth, D.L. and Ngobi, G., 1992. Hydrogeologic  
390 Evaluation Of Fracture Permeability In Crystalline Basement Aquifers Of Uganda.  
391 *Hydrogeology Journal*, 1(1): 55-65.

392 Kruseman, G.P. and Ridder, N.A., 1990. Analysis and evaluation of pumping test data. ILRI  
393 Publication., 377 pp.

394 Maréchal, J.C., 2009. Editor's message: the *sunk cost fallacy* of deep drilling. *Hydrogeology*  
395 *Journal*, 18: 287-289, doi: 10.1007/s10040-009-0515-2.

396 Maréchal, J.C., Dewandel, B., Galeazzi, L., Bournet, G. and Ahmed, S., 2006. Combined  
397 estimation of specific yield and natural recharge in a semi-arid groundwater basin with  
398 irrigated agriculture. *Journal of Hydrology*, 329(1-2): 281-293.

399 Maréchal, J.C., Dewandel, B. and Subrahmanyam, K., 2004. Use of hydraulic tests at  
400 different scales to characterize fracture network properties in the weathered-fractured  
401 layer of a hard rock aquifer. *Water Resources Research*, 40(11).

402 Massuel, S., Perrin, J., Wajid, M., Mascré, C. and Dewandel, B., 2009. A Simple, Low-Cost  
403 Method to Monitor Duration of Ground Water Pumping. *Ground Water*, 47(1): 141-  
404 145.

405 Mayo, A.L., Morris, T.H., Peltier, S., Petersen, E.C., Payne, K., Holman, L.S., Tingey, D.,  
406 Fogel, T., Black, B.J., Gibbs, T.D. (2003) Active and inactive groundwater flow  
407 systems: evidence from a stratified, mountainous terrain. *GSA Bull* 115(12):1456-  
408 1472

409 Moyen, J.F., Martin, H. and Jayananda, M., 2001. Multi- element geochemical modeling of  
410 crust-mantle interactions during late-Archean crustal growth: the Closepet Granite  
411 (South India). *Precambrian Research*, 112: 87-105.

412 Neuman, S.P., 1975. Analysis of Pumping Test Data From Anisotropic Unconfined Aquifers  
413 Considering Delayed Gravity Response. *Water Resources Research*, 11(2): 329-342.

414 Paillet, F.L., 1998. Flow modeling and permeability estimation using borehole flow logs in  
415 heterogeneous fractured formations. *Water Resources Research*, 34(5): 997-1010.

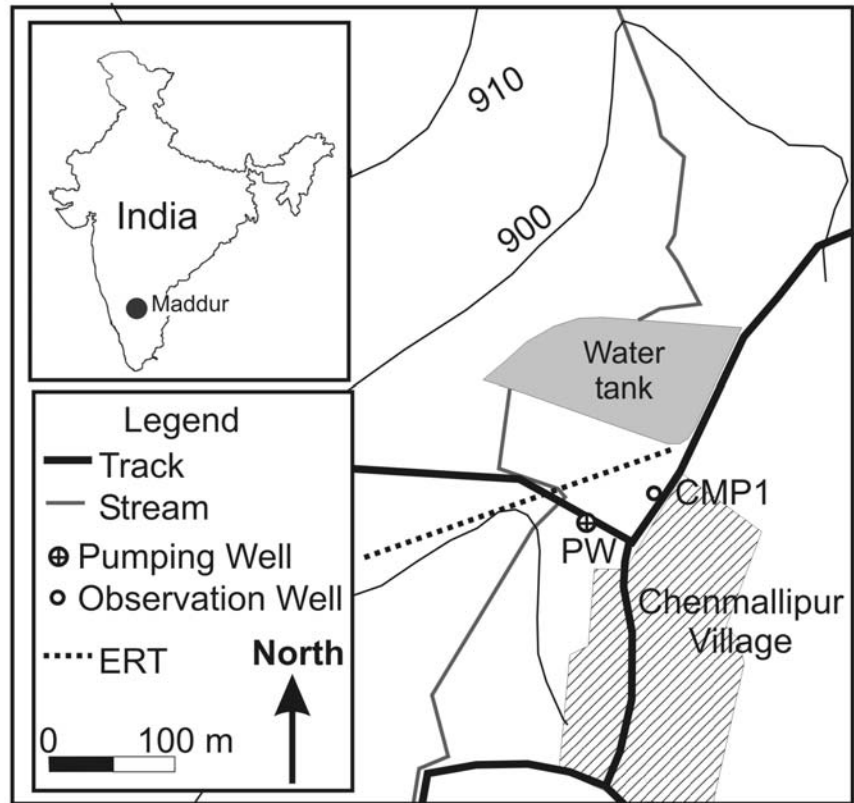
416 Taylor, R. and Howard, K., 2000. A tectono-geomorphic model of the hydrogeology of  
417 deeply weathered crystalline rock: Evidence from Uganda. *Hydrogeology Journal*,  
418 8(3): 279-294.

419 Theis, C.V. 1935. The relationship between the lowering of the piezometric surface and the  
420 rate and duration of discharge of a well using groundwater storage. *Eos Trans. AGU*,  
421 16, 519.

422

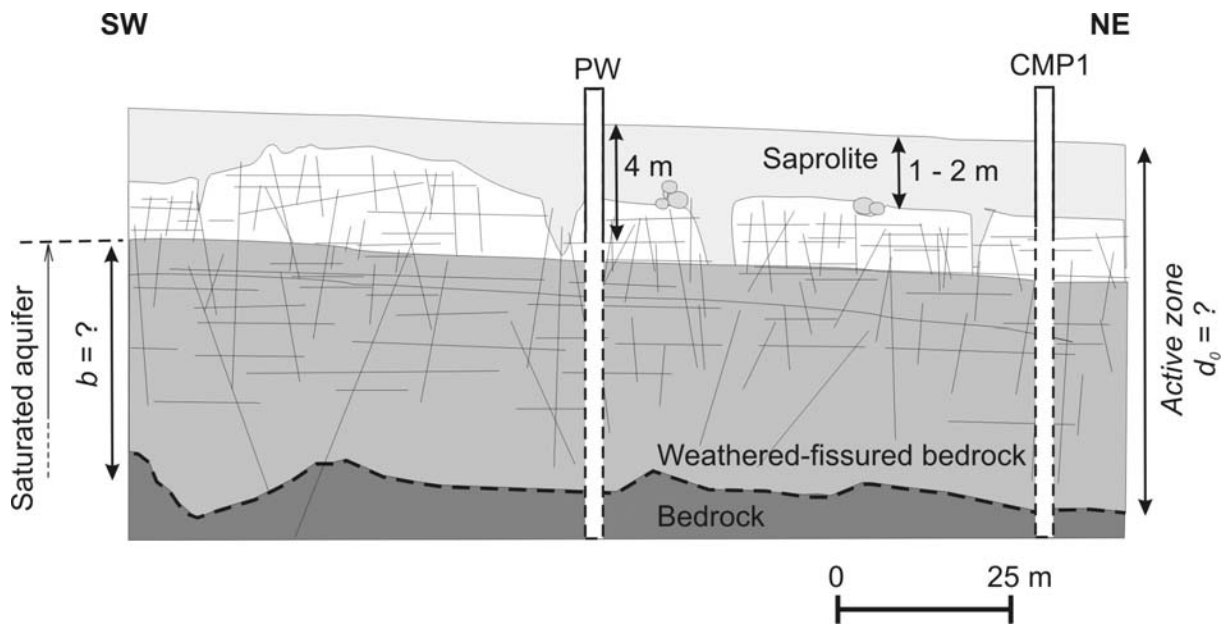
423

424 **Figures**  
425



426  
427  
428  
429  
430

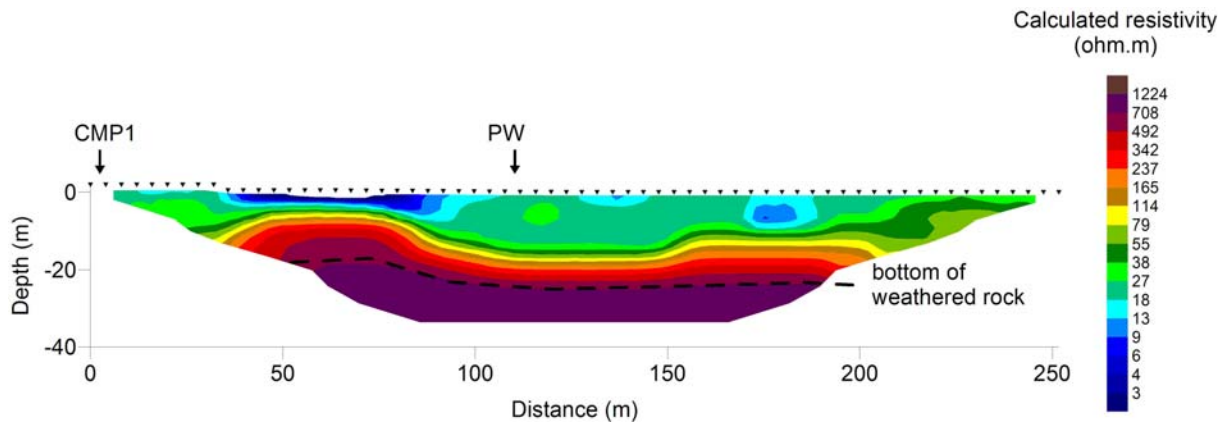
Figure 1: Location of the multiple pumping tests experimental site and the electrical resistivity tomography (ERT) profile in Maddur watershed



431  
432

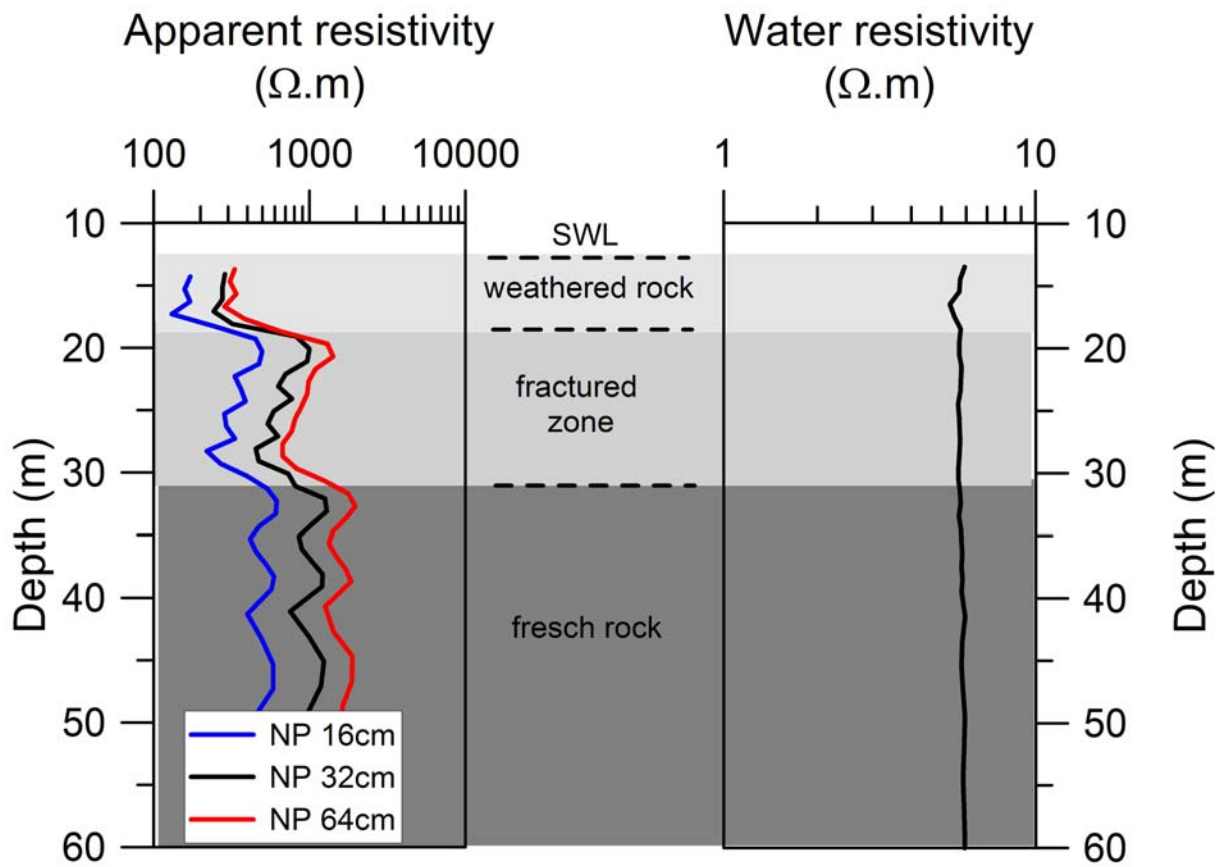
Figure 2: Hydrogeological section of the pumping site ( $d_0$ : depth to the bottom of the aquifer)

433



434

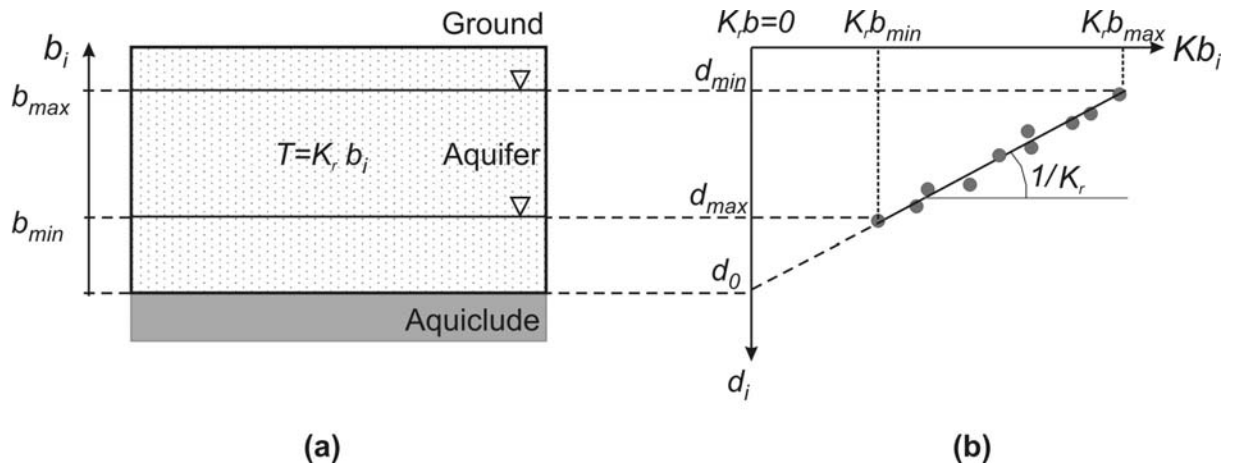
435 Figure 3: Electrical resistivity tomography (ERT) results



436

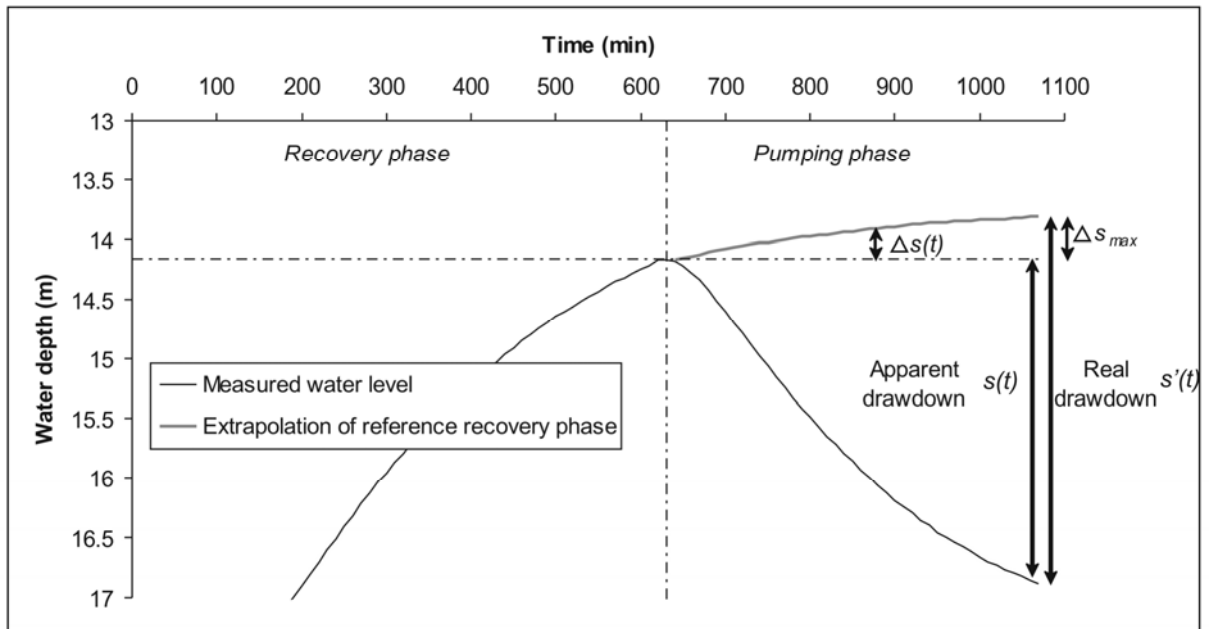
437 Figure 4: Electrical logging (CMP1, NP16, NP32 and NP64 are the lengths in cm of the used  
438 probe)

439



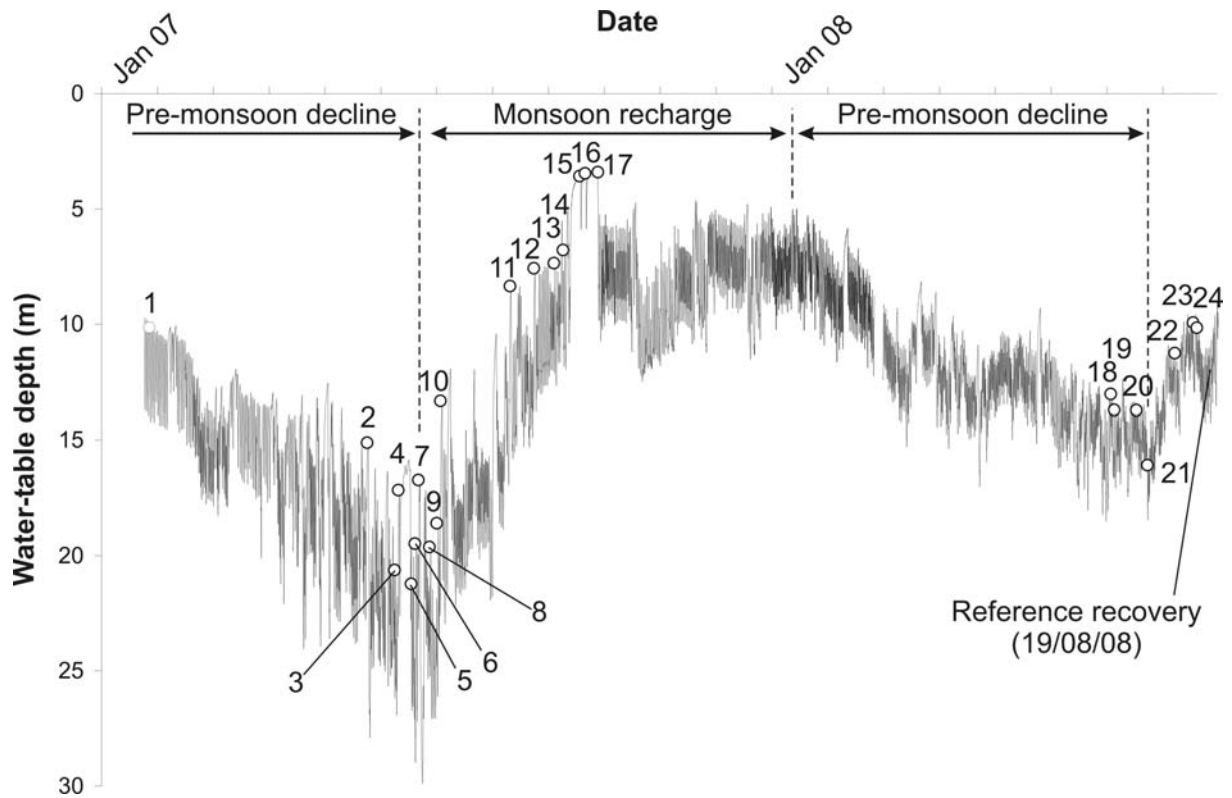
440  
441  
442  
443

Figure 5: (a) Unconfined aquifer with variable initial conditions of saturated thickness  $b_i$  (b) linear decrease of transmissivity with depth to water table;  $d_i$  is the depth to water table

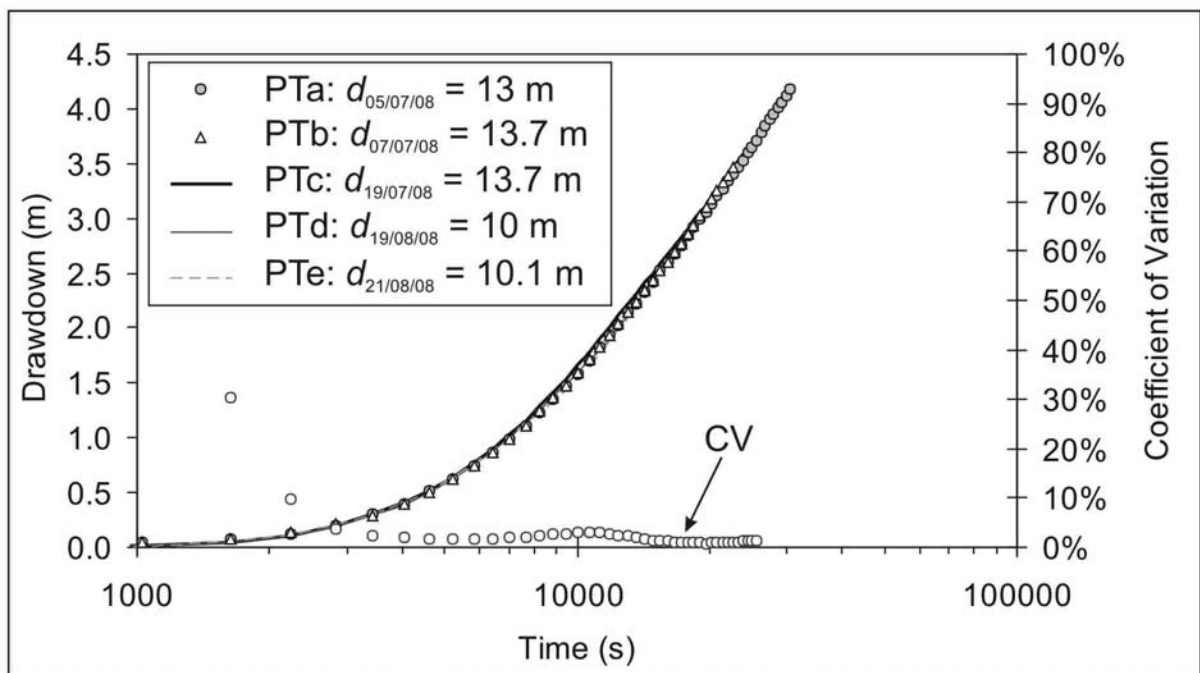


444  
445  
446

Figure 6: Example of a drawdown corrected with respect to the recovery effect

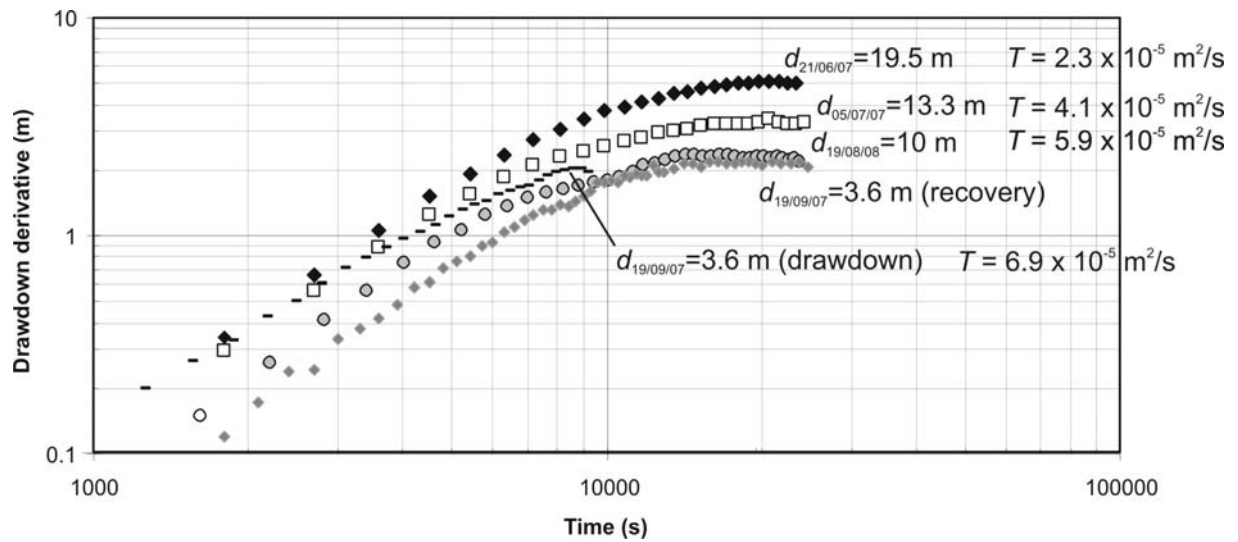


447  
 448 Figure 7: Water-table depth fluctuations at CMP1 during the monitoring period (analyzed  
 449 pumping cycles are numbered according to Table 2).

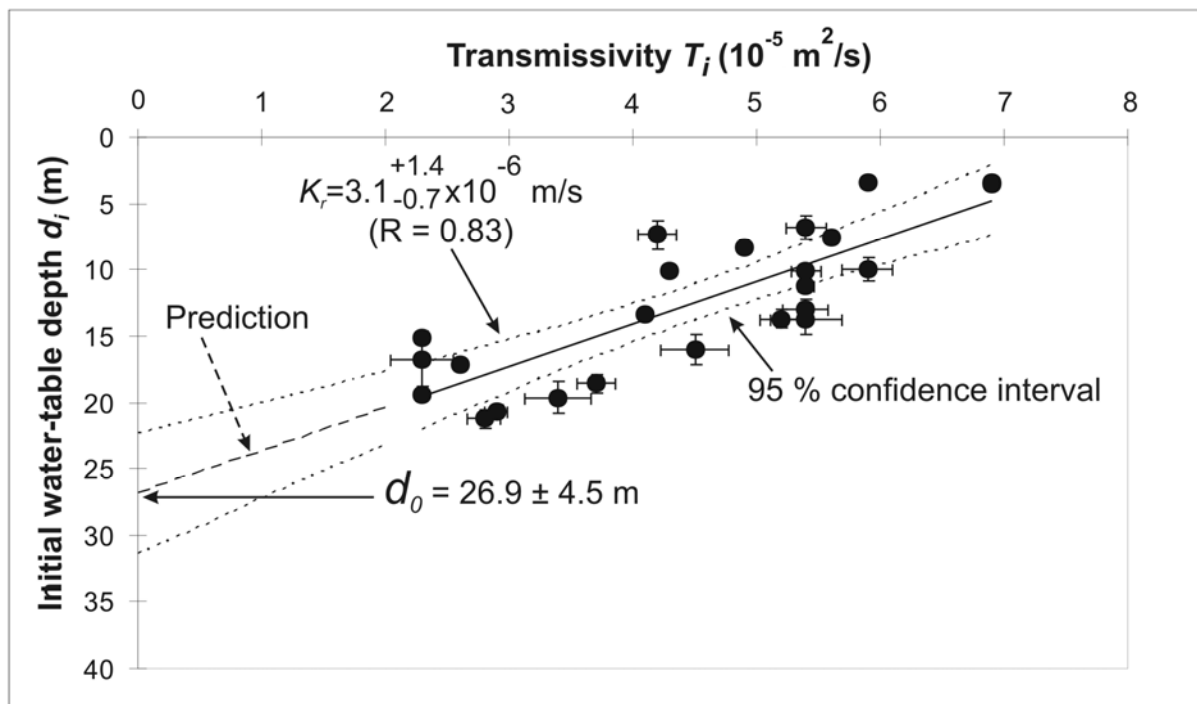


450  
 451 Figure 8: Corrected drawdown at CMP1 well during five pumping tests (PT) between 5th July  
 452 and 21st August 2008, with similar initial conditions (initial water-level depth  $d$   
 453 ranging from 10 to 14 m)

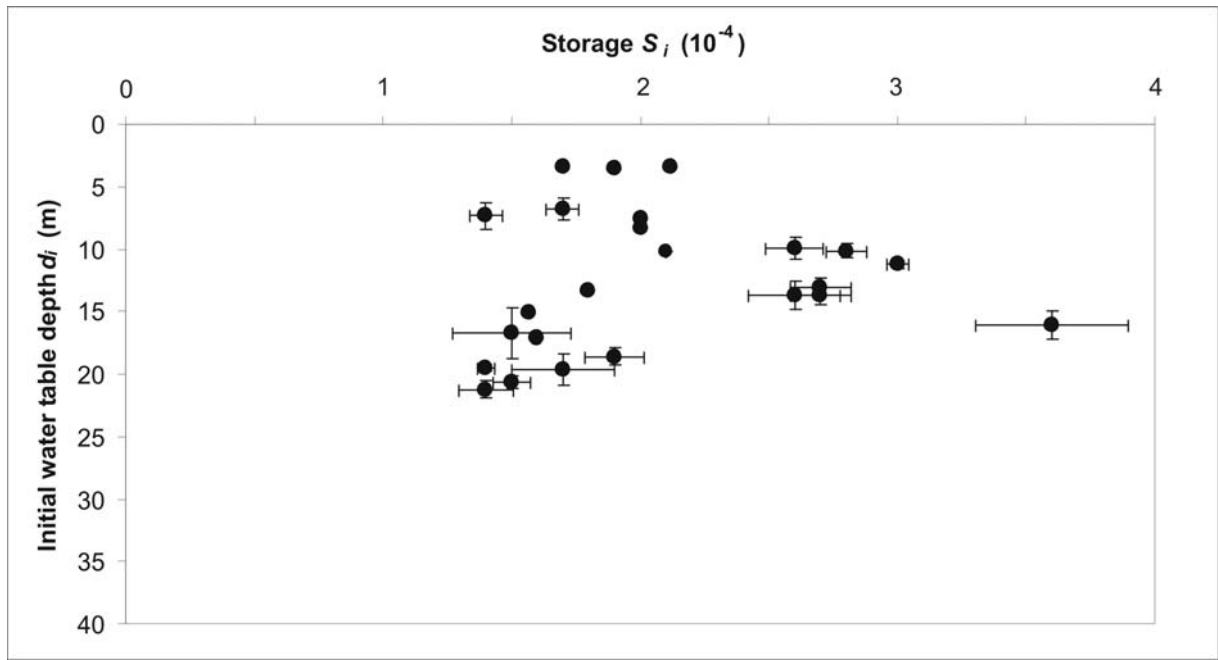
454



455  
 456 Figure 9: Drawdown derivative of several pumping cycles starting with variable initial water-  
 457 table depths  
 458



459  
 460 Figure 10: Transmissivity obtained from multiple pumping tests at CMP1 as a function of  
 461 initial water-table depth



462

463 Figure 11: Storage coefficient obtained from multiple pumping tests at CMP1 as a function of  
 464 initial water-table depth

465

466

467 **Tables**

468

469 **Table 1: Characteristics of monitored wells**

470

Well	Type	Diameter (m)	Depth (m)	Distance to PW (m)	Monitoring device
PW	Pumping well	0.165	> 50	-	Thermochron iButton
CMP1	Observation well	0.165	72	66	Water level data logger

471

472

473

474 **Table 2: Results of the interpretation of  $n = 24$  pumping cycles at CMP1 using the Neuman model.  $i$  is the**

475 **pumping cycle number (see Figure 7).  $T_i$  and  $S_i$  respectively transmissivity and storage coefficient**

476 **calculated from  $i^{\text{th}}$  pumping cycle.**

477

$i$	Date	Initial water- table depth $d_i$ (m)	$T_i$ ( $10^{-5}$ m <sup>2</sup> /s)	$S_i$ ( $10^{-4}$ )
1	27/01/2007	10.14	4.3	2.1
2	26/05/2007	15.12	2.3	1.6
3	10/06/2007	20.63	2.9	1.5
4	12/06/2007	17.17	2.6	1.6
5	19/06/2007	21.23	2.8	1.4
6	21/06/2007	19.49	2.3	1.4
7	23/06/2007	16.73	2.3	1.5
8	29/06/2007	19.63	3.4	1.7
9	03/07/2007	18.60	3.7	1.9
10	05/07/2007	13.33	4.1	1.8
11	12/08/2007	8.35	4.9	2.0
12	25/08/2007	7.57	5.6	2.0
13	05/09/2007	7.35	4.2	1.4
14	10/09/2007	6.78	5.4	1.7
15	19/09/2007	3.58	6.9	1.9
16	22/09/2007	3.45	6.9	2.1
17	29/09/2007	3.40	5.9	1.7
18	05/07/2008	13.02	5.4	2.7
19	07/07/2008	13.71	5.2	2.7
20	19/07/2008	13.72	5.4	2.6
21	25/07/2008	16.08	4.5	3.6
22	09/08/2008	11.25	5.4	3.0

23	19/08/2008	9.93	5.9	2.6
24	21/08/2008	10.15	5.4	2.8
	<b>Average</b>	<b>12.52</b>	<b>4.5</b>	<b>2.1</b>
	<b>Standard deviation</b>	<b>5.5</b>	<b>1.4</b>	<b>0.06</b>
	<b>Coefficient of variation</b>	<b>0.44</b>	<b>0.32</b>	<b>0.29</b>

478